Energy Conversion and Management: X 24 (2024) 100746

Contents lists available at ScienceDirect

Energy Conversion and Management: X

journal homepage: www.sciencedirect.com/journal/energy-conversion-and-management-x

Vapor-feed direct methanol fuel cells using pure methanol

Ryan Spragg [a], Xianglin Li [a,b,*]

[a] Department of Mechanical Engineering and Materials Science, Washington University in St. Louis, St. Louis, MO 63130, USA
[b] Department of Mechanical Engineering, University of Kansas, Lawrence, KS 66045, USA

ARTICLE INFO

Keywords:
DMFC
Pure methanol
Water management
Methanol crossover
Energy density
Liquid-vapor two-phase flow

ABSTRACT

This work optimizes the performance of the direct methanol fuel cell (DMFC) to increase its efficiency and strengthen its validity in portable power generation. Specifically, this work focuses on optimizing vapor-feed supply techniques and incorporating water management layers (WMLs) to analyze their effect on methanol crossover. The significance of the vapor-feed supply technique is to enhance the reaction kinetics of the methanol oxidation reaction (MOR) and enable the use of pure methanol (MeOH) as a fuel. Pure methanol is the ideal fuel for the DMFC as it has the highest possible energy density compared to dilute concentrations. However, use of pure methanol is hindered by methanol crossover, which is regarded as the largest technical barrier to commercializing DMFCs. This study measured methanol crossover through a CO_2 sensor attached to the cathode outlet and added hydrophobic WMLs to the cathode to alleviate the methanol crossover. The hydrophobic WMLs increased the mass transfer resistance to generate a pressure gradient that encourages water backflow for use in both the proton exchange membrane (PEM) and anode reactions. The influence of vapor flow rate and fuel concentration will also be explored to show their impact on performance and methanol crossover. Likewise, long-term consumption and durability tests were conducted with and without a WML to dictate the WML's superior fuel efficiency, total efficiency, energy density, and reduced methanol crossover using pure methanol. The addition of the WML increased the energy density of the vapor feed DMFC, using pure methanol, from 705.9 Wh kg^{-1}_{MeOH} to 867.7 Wh kg^{-1}_{MeOH} and lowered the crossover current density by 14.8 % when discharged at a constant 200 mA cm^{-2}.

1. Introduction

The DMFC is a proton exchange membrane fuel cell (PEMFC) that utilizes methanol (MeOH) fuel as a hydrogen carrier. Liquid methanol is fed into the anode, and air is supplied into the cathode. The fuel on the anode undergoes a methanol oxidation reaction (MOR), which is supported by a platinum-ruthenium (PtRu) catalyst:

$$CH_3OH + H_2O \rightarrow 6H^+ + 6e^- + CO_2 \tag{1}$$

The hydrogen ions transport across the proton exchange membrane (PEM) to the cathode, where they combine with oxygen from the air, through an oxygen reduction reaction (ORR), facilitated by a platinum (Pt) catalyst:

$$\frac{3}{2}O_2 + 6H^+ + 6e^- \rightarrow 3H_2O \tag{2}$$

These two half-reactions contribute to the global reaction of the DMFC:

$$CH_3OH + \frac{3}{2}O_2 \rightarrow 2H_2O + CO_2 \tag{3}$$

As hydrogen ions transport through the PEM, the electrons are transported through an external circuit, generating current, and powering electronic devices.

The DMFC holds multiple advantages over other sources of power generation. Recently, technological advancements in power generation sources have focused on reducing or eliminating CO_2 emissions. Although the DMFC produces a similar amount of CO_2 to gasoline, on an energy basis, it is a biofuel that can be produced from multiple renewable sources. Methanol has a high theoretical gravimetric energy density, 6,100 Wh kg^{-1}. However, the DMFC's reported operational efficiency in the literature is limited to 20 %, yielding a theoretical energy density of 1,220 Wh kg^{-1}, which is still much higher than current lithium-ion battery technology at 250 Wh kg^{-1} [1]. Likewise, methanol has a higher volumetric energy density of 4,400 Wh/L than hydrogen's volumetric energy density of 1,555 Wh/L when compressed at 700 bar [2,3]. The DMFC yields high energy density and efficiency for light-duty

* Corresponding author.
E-mail address: lxianglin@wustl.edu (X. Li).

https://doi.org/10.1016/j.ecmx.2024.100746
Received 7 August 2024; Received in revised form 23 September 2024; Accepted 1 October 2024
Available online 4 October 2024

Nomenclature

Acronym	Definition
CC	Carbon Cloth
DI	Deionized
FML	Fuel Management Layer
GDL	Gas Diffusion Layer
HFR	High-Frequency Resistance
IPA	Isopropyl Alcohol
LFDMFC	Liquid Feed Direct Methanol Fuel Cell
MCO	Methanol Crossover
MEA	Membrane Electrode Assembly
MeOH	Methanol
MOR	Methanol Oxidation Reaction
MPL	Microporous Layer
N_2	Nitrogen
OCV	Open Circuit Voltage
ORR	Oxygen Reduction Reaction
PEM	Proton Exchange Membrane
PEMFC	Proton Exchange Membrane Fuel Cell
PPD	Peak Power Density
Pt	Platinum
PtRu	Platinum-Ruthenium
PTFE	Polytetrafluoroethylene
RH	Relative Humidity
TKK	Tanaka Precious Metals
VFDMFC	Vapor Feed Direct Methanol Fuel Cell
WML	Water Management Layer
Variable	Definition, Units
A	Area, Cm^2
c_{fuel}	Fuel Concentration, Mol L^{-1}
Δ_{Mass}	Mass Change, g
Δ_{Time}	Test Time, Hours
F	Faraday's constant, C mol^{-1}
i	Current Density, mA cm^{-2}
i_{MCO}	Methanol Crossover Current Density, mA cm^{-2}
M_{MeOH}	Molar Mass of Methanol, G mol^{-1}
n	Number of Electrons, N/A
η_{tot}	Cell Efficiency, %
η_{fuel}	Fuel Efficiency, %
η_{volt}	Voltage Efficiency, %
$\dot{n}_{CO_2}$	Flow Rate of CO_2, mol s^{-1}
$\dot{n}_{MeOH\ AN}$	Anode Flow Rate of Methanol, mol s^{-1}
$\dot{n}_{MeOH\ CA}$	Cathode Flow Rate of Methanol, mol s^{-1}
P_{atm}	Atmospheric pressure, kPa
P_{MeOH}	Partial Pressure of Methanol, kPa
$P_{Partial}$	Partial Pressure, kPa
P_{Sat}	Saturation Pressure, kPa
P	Pressure, kPa
$\dot{Q}_{Air}$	Air Flow Rate, L min^{-1}
$\dot{Q}_{MeOH\ Consumption}$	Methanol Consumption Rate, mol s^{-1}
$\dot{Q}_{MeOH\ Supply}$	Methanol Supply Rate, mol s^{-1}
$\dot{Q}_{MeOH\ TS}$	Tested Methanol Supply Rate, mol s^{-1}
$\dot{Q}_{N2}$	Flow Rate of Nitrogen, mL min^{-1}
R	Universal Gas Constant, J mol^{-1} K^{-1}
SR_{Tested}	Tested Stoichiometric Ratio, N/A
$SR_{Theoretical\ Liq}$	Theoretical Liquid Feed Stoichiometric Ratio, N/A
$SR_{Theoretical\ Vap}$	Theoretical Vapor Feed Stoichiometric Ratio, N/A
T	Temperature, K
U_{MeOH}	Methanol Energy Density, Wh kg^{-1}
U_{tot}	Total Energy Density, Wh kg_{MeOH}^{-1}
V_{avg}	Average Voltage, V
$V_{Theoretical}$	Theoretical Voltage, V
y_{CO_2}	CO_2 Concentration, %

transportation and mobile applications. For example, Ahmed et al. summarized the performance of a DMFC under various operating conditions and their improvements to the efficiency of a portable military power device, Jenny 600 s [4]. Although hydrogen is seen as a more suitable fuel in the long term, current production, storage, and transportation prevent hydrogen's large-scale adoption in fuel cell technology. Furthermore, hydrogen gas is highly volatile and risks explosion if not stored and transported properly. On the other hand, methanol can be stored as a liquid at ambient temperature and pressure. Despite this, methanol is toxic and flammable, posing risks if improperly managed.

1.1. Vapor-feed direct methanol fuel cells

Typically, low-concentration methanol solutions are used in commercial and research applications for DMFCs to maintain a low methanol crossover rate. Methanol crossover (MCO) is the phenomenon that occurs when methanol diffuses through the PEM from the anode to the cathode, due to the concentration difference, and reacts directly with the oxygen on the cathode. This creates a mixed voltage potential, which lowers efficiency and accelerates the degradation of the membrane electrode assembly (MEA). Dilute solutions are useful in a liquid-feed direct methanol fuel cell (LFDMFC) due to the low MCO. Although the two-phase nature of an LFDMFC has been extensively studied [5], a vapor-feed direct methanol fuel cell (VFDMFC) drastically improves the MOR due to methanol's increased mass diffusivity in a gaseous phase [6]. Multiple comprehensive reviews of the vaporization methods of the vapor feed DMFC, optimal cell design, passive versus active operation, and the disadvantages caused by methanol crossover and insufficient water management have been explored [7–9]. The performance and design of VFDMFCs using high concentrations of methanol fuel have also been extensively studied using active and passive supply techniques [10–16]. Eccarius et. al discovered the effect of parameters such as gas diffusion media, fuel concentration, and operating conditions on a passive DMFC and how an optimal design can improve efficiency [10]. Kim used porous foam, vaporizer, barrier, and buffer layers to modify the vapor transport of liquid-supplied methanol, leading to a 70 % higher fuel efficiency and 1.5 times higher energy density than a passive LFDMFC [11]. Li et. al tested porous PTFE methanol barrier layers and electrolytes with various thicknesses and fuel concentrations and found that a semi-passive VFDMFC could produce 115.8 mW cm^{-2} using a 20 mol/L fuel concentration [12]. Xu et. al tested various dry air flow rates and temperatures on an active DMFC fed with neat methanol and noted a large performance decline, when testing at 70 °C and using 20 sccm of air flow, after a constant current discharge at 50 mA cm^{-2} for more than 90 min [13]. More recently, Moreno-Zuria et. al used a filter paper electrolyte with a constant flow of potassium hydroxide to vaporize neat methanol in a micro-VFDMFC stack to power multiple LEDs. This addition led to a stable 28 hrs. of operation at a constant voltage of 0.35 V[14].

1.2. Water management layers

Despite these promising results, the largest challenge for the VFDMFC is the lack of available water in the anode to hydrate the PEM and contribute to the MOR, especially when using highly concentrated fuels. Water management in a VFDMFC is critical, and the use of additional WMLs has improved the backflow of water from the cathode into the PEM and anode [17–19] Li et al. incorporated a WML to the cathode

with various open area ratios and found an optimal open area ratio of 20 % produced 118.9 mA cm^{-2} of current density and 22.7 mW cm^{-2} of power density when supplying neat methanol passively in a VFDMFC [17]. Zhang et al. investigated the vapor–liquid equilibrium of various carbon materials through condensation and evaporation experiments. Out of all the nitrogen-doped materials tested, including carbon black, carbon nanotubes, and mesoporous carbon, it was found that carbon aerogel had the smallest pore size, lowest evaporation rate, and highest condensation rate. The Kelvin equation explained the measured vapor–liquid equilibrium of these materials, which made carbon aerogel an ideal material to act as a WML as it decreased the vapor pressure of water vapor in the diffusion layer back into a liquid state [18]. Xu et. al [19] used two carbon cloths with 50 wt% PTFE treatment as a WML and a PTFE sheet as an air filter layer on the cathode, which produced the superior power density of any configuration at 33 mW cm^{-2} in a passive VFDMFC using neat methanol. Besides including WMLs, many other design approaches have been taken to improve water retention. Zhang et al. used a quasi-superhydrophobic sintered porous metal plate on the cathode to improve performance and reduce crossover when neat methanol was supplied passively [20]. These include MPL resistivity and pore structure optimization [21], a super hydrophilic cathode current collector [22], mass transport analysis of water in an MEA [23], and the influence of MEA thickness on water transport in the cathode at various temperatures [24]. Oppositely, efforts have been made to improve the characteristics of the anode to achieve a similar outcome caused by using a WML on the cathode. Most notably, carbon aerogel was used as an FML [25], and anode gas diffusion layers (GDLs) were used after various hydrophilic and hydrophobic treatments [26]. Likewise, Wu et. al developed a sandwich structured membrane using an ultra-thin reaction layer comprised of PtRu catalyst, SiO_2, and Nafion ionomer sandwiched between two membranes promoting a reaction between methanol and oxygen in the reaction layer in order to reduce the transport distance of water in a neat methanol DFMC. This addition led to a reduction in internal resistance from 0.08 mΩ to 0.06 mΩ when comparing a Nafion 212 membrane to a 0.1 mg_{PtRu} cm^{-2} sandwich membrane respectively [27].

1.3. Methanol crossover

While these approaches focus on generating water backflow, they all indirectly contribute to reducing MCO. Multiple studies have taken different approaches to include WMLs to reduce MCO experimentally. Li et al. experimentally measured water and methanol crossover in an LFDMFC by measuring the change in mass of a known fuel concentration as well as the change in concentration through FTIR [28]. Xu et al. found that two GDLs as a WML added to the cathode reduced both methanol and water crossover in a passive room temperature DMFC with 3 mol/L liquid fuel supplied. This led to a decrease in methanol-crossover flux from 0.002 to 0.001 mol $m^{-2}s^{-1}$ at a current density of 100 mA cm^{-2} [29]. Likewise, Jewett et al. studied several configurations using various thicknesses of Nafion membranes and 50 wt% PTFE-treated GDLs to act as a WML. Including two PTFE-treated GDLs and a Nafion 112 membrane resulted in a water balance coefficient of −1.71 compared to other configurations. This created reduced crossover and improved both the power density and efficiency of the cell using a 1 mol kg^{-1} solution of liquid fuel supplied passively [30]. This work aims to improve the peak power density and efficiency of an active VFDMFC by utilizing pure methanol as a fuel. This is achieved by testing various fuel concentrations and flow rates. Likewise, this study directly analyzed the effect that fuel concentrations and flow rates have on MCO. A CO_2 gas sensor will be incorporated into the cathode outlet to detect CO_2 generated by MCO, which will be converted to methanol crossover current density (i_{MCO}). The VFDMFC with a WML achieves a lower i_{MCO} which highlights its improved water retention while using pure methanol as a fuel. Most importantly, however, the use of WMLs enables the VFDMFC to use pure methanol as indicated through a series of long-term consumption tests that show increased efficiency and energy density.

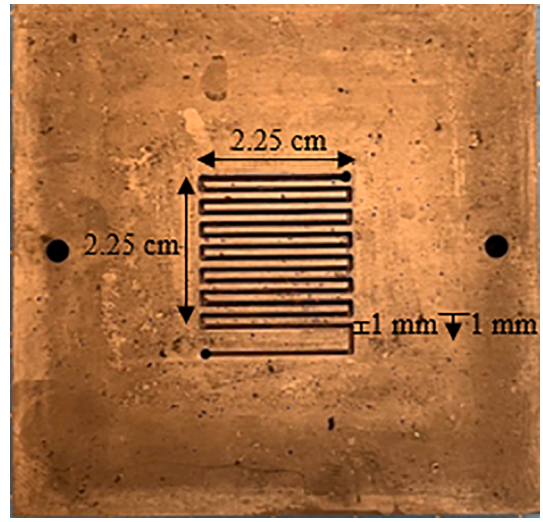

Fig. 1. 5 cm^2 serpentine flow channel.

2. Experimental setup

2.1. MEA fabrication

The catalyst ink for the anode is mixed using deionized (DI) water, isopropyl alcohol (IPA), TKK 77.4 % PtRu catalyst, and Nafion 5 wt% ionomer. A one-to-one ratio of DI water: IPA was added, and appropriate amounts of Nafion and PtRu were added to achieve an ionomer to PtRu ratio of 0.4. Likewise, the cathode catalyst ink uses similar ingredients, except the catalyst is solely TKK 57.7 % Pt. Similarly, the DI to IPA ratio was one-to-one, and the ionomer to Pt ratio for the cathode was 0.4. Both inks are sonicated in a Branson 1800 Sonicator for 30 min to ensure appropriate particle dispersion. The sonicated ink is then transferred into an Iwata Ninja Jet airbrush. The anode catalyst is spray-coated onto a Sigracet 22BB carbon paper substrate with a 5 wt% hydrophobic microporous layer (MPL) until a catalyst loading of 4.5 mg_{PtRu} cm^{-2} is achieved. Similarly, the cathode is spray-coated onto a CT W1S1011 Carbon Cloth (CC) substrate with a 5 wt% PTFE MPL until a loading of 1.5 mg_{Pt} cm^{-2}. The anode and cathode are assembled along with a Nafion 212 membrane. These components are placed and aligned in a PTFE gasket covered in aluminum foil and are hot pressed at 135 °C using a Carver 4386 Hot Press under 1 Ton of force for 5 min. The tests that include a WML use the same CT W1S1011 CC with a 5 wt% PTFE MPL from the fuel cell store, product code 23070001. The CC was cut to the same size, 5 cm^2, as the active area for the MEA and is placed between the cathode substrate and the cathode flow channel with the MPL facing away from the flow channel to encourage a favorable pressure gradient to capture water generated from the ORR.

2.2. MEA activation

A Scribner 890e Fuel Cell Test System is used in conjunction with a 5 cm^2 serpentine flow channel Scribner Fuel Cell Test Frame to test all MEAs. The dimensions of the serpentine flow channel are shown in Fig. 1 and are used in all subsequent tests. The fuel cell is heated to 60 °C using a cartridge heater inserted into the fuel cell endplates and is controlled by a PID temperature controller embedded into the Scribner 890e Fuel Cell Test System. The anode is fed with a 0.25 mol/L (0.81 wt%) liquid solution of methanol and DI water at a flow rate of 1 mL min^{-1} using a CorSolutions PnueWave Pump. Air is fully humidified by dispensing air into a bottle of DI water, which sits in a FischerBrand™ Isotemp™ Heated Bath Circulator set to 80 °C. The air is supplied using a Cole-

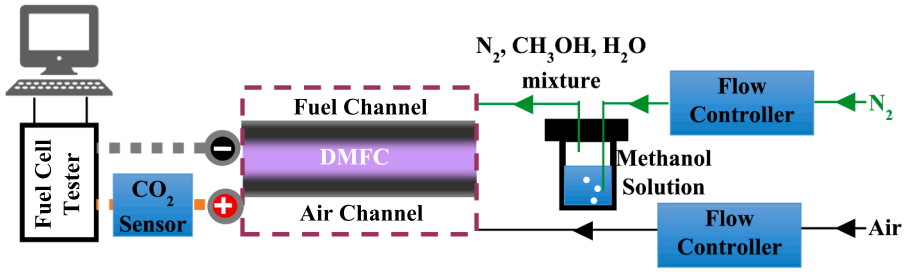

Fig. 2. VFDMFC system layout.

Parmer® 32907–67 Flowmeter at a flow rate of 200 mL min^{-1}. Initially, the cell is held at open circuit voltage (OCV) for 5 min to ensure it has stabilized. Next, a polarization scan is conducted by decreasing the voltage from OCV to a final voltage of 0.2 V in increments of 25 mV. Lastly, the cell is held at a constant voltage of 0.3 V for 30 min, and the process repeats 6 times or until the performance stabilizes.

2.3. MEA performance tests

Each MEA was tested using a baseline 1 mol/L (3.2 wt%) concentration of liquid-fed methanol at room temperature (22 °C +/- 1 °C) and fully humidified air, 100 % relative humidity (RH). Like activation testing, each performance test is conducted by holding the cell at OCV for 5 min, then the cell is scanned from OCV to 0.2 V in increments of 25 mV. Three performance scans are conducted to ensure stable performance. For the vapor-feed system, an AirGas tank of research-grade Nitrogen (N_2) was connected to a Masterflex® Proprtial Flowmeter Controller with +/- 0.8 % accuracy and set to atmospheric pressure (101.325 kPa). The flow meter is then connected to a bottle of methanol fuel kept at room temperature (22 °C +/- 1 °C), and the desired flow rate is set. N_2 is then bubbled into the fuel bottle, vaporizing the methanol through a concentration gradient and driving the fuel into the anode chamber. Fig. 2 gives a schematic breakdown of the VFDMFC. An important criterion for further understanding DMFC performance is the stoichiometric ratio ($SR_{\text{Theoretical Vap}}$). This is defined as the ratio between the methanol supply rate ($\dot{Q}_{\text{MeOH Supply Vap}}$) of vaporized methanol and the methanol consumption rate ($\dot{Q}_{\text{MeOH Consumption}}$) of methanol. In an ideal case, the stoichiometric ratio would be exactly 1 at any instance, meaning our supply rate is sufficient compared to our consumption rate to avoid fuel starvation. Conversely, a stoichiometric ratio between 1 and 2 would reduce an oversupply of fuel, drastically improving fuel efficiency and energy density. This criterion will be used to determine appropriate fuel flow rates for both the liquid and vapor feed systems, and for increasing fuel efficiency. Please note that $SR_{\text{Theoretical Vap}}$ is also equivalent to the inverse of theoretical fuel efficiency. The tested fuel efficiency (η_{fuel}) will be based on the inverse of our tested stoichiometric ratio discussed in ***Section 2.4***. The $\dot{Q}_{\text{MeOH Supply Vap}}$ is highly dependent on the volumetric flow rate of N_2 supply into the methanol bottle, $\dot{Q}_{N2}$ as well as the partial pressure of methanol, P_{MeOH}, at room temperature (22 °C):

$$\dot{Q}_{\text{MeOH Supply Vap}} = \frac{\dot{Q}_{N2} \times P_{\text{MeOH}}}{P_{\text{atm}}} \tag{4}$$

P_{atm} is the atmospheric pressure. The $\dot{Q}_{\text{MeOH Consumption}}$ is dependent on the operating current density i.

$$\dot{Q}_{\text{MeOH Consumption}} = \frac{i \times A}{n \times F} \tag{5}$$

A is the active area of the MEA n equals 6 and is the number of electrons produced by each methanol molecule from the MOR and F is Faraday's constant, which is 96,485C/mol. The resulting theoretical stoichiometric ratio is:

$$SR_{\text{Theoretical Vap}} = \frac{\dot{Q}_{\text{MeOH Supply Vap}}}{\dot{Q}_{\text{MeOH Consumption}}} \tag{6}$$

The stoichiometric ratio is also be used for the liquid feed case. The supply rate of liquid feed methanol ($\dot{Q}_{\text{MeOH Supply Liq}}$) is dependent on the concentration of the fuel (c_{fuel}) and the anode molar flow rate of methanol ($\dot{n}_{\text{MeOH AN}}$).

$$\dot{Q}_{\text{MeOH Supply Liq}} = \dot{n}_{\text{MeOH AN}} \times c_{fuel} \tag{7}$$

The liquid feed stoichiometric ratio ($SR_{\text{Theoretical Liq}}$) can be calculated similarly to the $SR_{\text{Theoretical Vap}}$ given the consumption rate of methanol does not depend on the fuel's state of matter.

$$SR_{\text{Theoretical Liq}} = \frac{\dot{Q}_{\text{MeOH Supply Liq}}}{\dot{Q}_{\text{MeOH Consumption}}} \tag{9}$$

2.4. MEA consumption testing procedure

For each test, an initial amount of pure methanol was weighed using an Acuris Instruments W3100A-210 Analytical Balance with +/- 0.2 mg accuracy within the bottle and its tubing connections. Next, the bottle was connected to the flowmeter mentioned in ***Section 2.3***, to drive the vaporized methanol into the DMFC. Once all connections were secured, the flow meter was turned on and set to 15 mL min^{-1} when testing at 100 mA cm^{-2}, and 25 mL min^{-1} when testing at 200 mA cm^{-2}, these flow rates will be discussed in ***Section 3.5***. The anode fuel bottle sat at room temperature (22 °C), and the cathode air bottle sat at 100 % RH. Next, the cell sat at OCV for 5 min to stabilize. Then, the cell was set to a fixed current of 0.5 A and 1 A for the 100 mA cm^{-2} and 200 mA cm^{-2} tests, respectively, for > 14 h. The FuelCell® software recorded current density, voltage, power density, and HFR throughout the test. Once all tests were completed, the flow controller was unplugged to prevent excess fuel from vaporizing and ensure an accurate mass change. The fuel bottle and its tubing connections were placed back onto the analytical balance and the mass was recorded. To determine the efficiency, the mass difference was taken between the start and end of the test. The test supply rate ($\dot{Q}_{\text{MeOH TS}}$) is based on the mass consumed (Δ_{Mass}), the molar mass of methanol (M_{MeOH}), and test time (Δ_{Time}):

$$\dot{Q}_{\text{MeOH TS}} = \frac{\frac{\Delta_{\text{Mass}}}{M_{\text{MeOH}}}}{\Delta_{\text{Time}}} \tag{9}$$

This allows for the calculation of the tested stoichiometric ratio:

$$SR_{\text{Tested}} = \frac{\dot{Q}_{\text{MeOH TS}}}{\dot{Q}_{\text{MeOH Consumption}}} \tag{10}$$

The fuel efficiency (η_{fuel}) is calculated by the ratio of $\dot{Q}_{\text{MeOH Consumption}}$ to $\dot{Q}_{\text{MeOH TS}}$, the fuel efficiency (η_{fuel}) is simply the inverse of the SR_{Tested}:

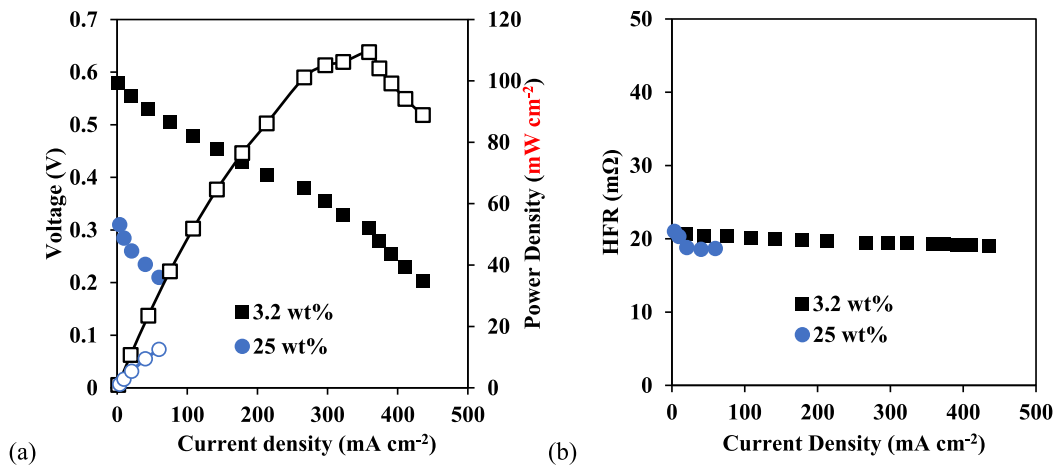

Fig. 3. (a) Performance of liquid feed DMFC using 3.2 wt% and 25 wt% fuel concentrations and (b) resulting HFR.

$$\eta_{\text{fuel}} = \frac{\dot{Q}_{\text{MeOH Consumption}}}{\dot{Q}_{\text{MeOH TS}}} \tag{11}$$

The voltage efficiency (η_{volt}) is calculated by the ratio of the average voltage (V_{avg}) to the theoretical voltage ($V_{\text{Theoretical}}$) of the DMFC which is 1.21 V [31]:

$$\eta_{\text{volt}} = \frac{V_{\text{avg}}}{V_{\text{Theoretical}}} \tag{12}$$

The voltage efficiency is calculated by the ratio of produced electrical energy to the energy supplied to the fuel cell, which also equals the fuel efficiency multiplied by the voltage efficiency:[32,33].

$$\eta_{\text{tot}} = \eta_{\text{fuel}} \times \eta_{\text{volt}} \tag{13}$$

Lastly, the energy density (U_{tot}) can be calculated by multiplying η_{tot} and the gravimetric energy density of methanol (U_{MeOH}) which is 6.1 kWh kg^{-1}.

$$U_{\text{tot}} = \eta_{\text{tot}} \times U_{\text{MeOH}} \tag{14}$$

2.5. Methanol crossover measurement

Methanol crossover rates are measured through the potentiostatic technique [34], gas chromatographic analysis [35], or with a CO_2 sensor or probe [36]. This study used a Sprint®IR-6 s CO_2 gas sensor with a +/- 5 % accuracy to determine the i_{MCO}. The fuel cell cathode outlet is connected to a Scribner Manual back-pressure device with built-in condensation capture tanks on the cathode. The CO_2 sensor was included at the downstream of the back pressure device. Residual water and water vapor exiting the fuel cell will be condensed into a liquid and captured in the back pressure device before the CO_2 sensor measures the exhaust gas. This leaves dry de-humidified air and CO_2 to pass across the sensor, ensuring an accurate reading. This also prevents any damage to the sensor from liquids or temperature. If a CO_2 percentage is detected on the cathode outlet flow stream, it would be evidence of crossover, given the MCO reaction is the same as **Eqn 3,** which produces CO_2 and H_2O. The Gas sensor collected data using the GasLab logging software in intervals of 1 min for an infinite period.

In ***Sections 3.3-3.4***, the cell sat at OCV for 1 h to ensure a stable reading from the CO_2 sensor. The final 20 min of collected data were averaged and used as the molar fraction of CO_2 (y_{CO_2}). With this information, the CO_2 flow rate on the cathode can be calculated:

$$\dot{n}_{CO_2} = \dot{n}_{\text{MeOH CA}} = \frac{y_{CO_2} \times P \times \dot{Q}_{\text{Air}}}{(R \times T)} \tag{15}$$

where $\dot{n}_{CO_2}$ is the molar flow rate of CO_2, $\dot{n}_{\text{MeOH CA}}$ is the molar flow rate of methanol at the cathode, $\dot{Q}_{\text{Air}}$ is air flow rate, P is the pressure of the cell, R is the universal gas constant, and T is the temperature at which the CO_2 data was collected. Since the crossover methanol faces extremely high overpotential in the cathode, all crossover methanol could be completely oxidized to CO_2. Therefore, the measured CO_2 flow rate can be considered as the methanol crossover rate. This allows for the calculation of the equivalent current density caused by MCO:

$$i_{\text{MCO}} = \frac{\dot{n}_{\text{MeOH CA}} \times n \times F}{A} \tag{16}$$

The variable n is the number of electrons produced by each methanol molecule from the MOR, A is the size of the MEA, and F is Faraday's constant.

3. Results and discussion

This study experimentally explored metrics such as liquid feed versus vapor feed supply, fuel concentration, and fuel flow rate. Most importantly, these metrics will be studied to enable pure methanol as a fuel coupled with a WML on the cathode to improve efficiency and energy density. Furthermore, all metrics were used to study their impact on the MCO rate using a Sprint®IR-6 s CO_2 Sensor incorporated into the cathode outlet. The performance is measured through traditional polarization and power density curves. Efficiency and energy density are evaluated through a series of long-term (>14 hrs) consumption tests at various fixed current densities.

3.1. Liquid feed concentration

The MEA was performance tested using the baseline 1 mol/L (3.2 wt %) solution, fed at 1 mL min-1, and was compared against a 25 wt% solution. The 25 wt% solution was fed into the DMFC at a flow rate of 0.33 mL min^{-1}. These flow rate selections are based on the $SR_{\text{Theorreical Liq}}$. Using **Eqns 5,7,** and **8** for the 3.2 wt% solution, the $SR_{\text{Theoretical Liq}}$ is 1.93 when $\dot{n}_{\text{MeOH AN}}$ is 1 mL min^{-1} and i is achievable 1 A cm^{-2}. The $SR_{\text{Theoretical Liq}}$ is similar to that of the $SR_{\text{Theoretical Vap}}$ case using 100 % pure methanol, 1.85 in Table 2, and satisfies the conditions described in ***Section 2.3***. The concentration of the liquid fuel solution had a strong impact on fuel cell performance and crossover.

The peak power density (PPD) decreases from 109.4 mW cm^{-2} to 12.5 mW cm^{-2} as the concentration increases from 3.2 wt% to 25 wt%. Although the ohmic resistance of the cell in Fig. 3b using 25 wt% fuel is 18.7 mΩ the methanol crossover current density (i_{MCO}) dominates the overall power reduction and limiting current density in Fig. 3**a**. The i_{MCO}

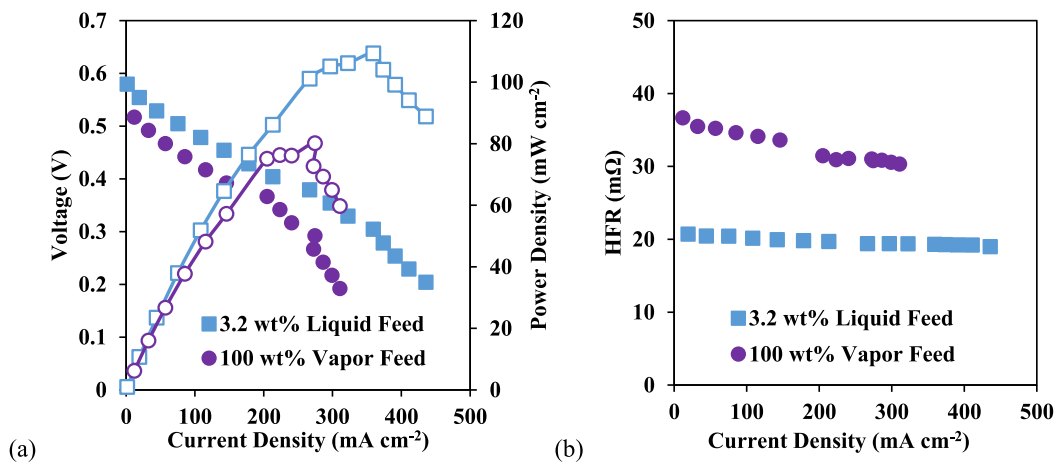

Fig. 4. Baseline testing performed at 60 °C using 3.2 wt% liquid feed and 100 wt% vapor feed: (a) polarization and power density curves and (b) HFR at 1 mL min^{-1} for 3.2 wt% and 30 mL min^{-1} for 100 wt%, 100 % RH, and 101.32 kPa.

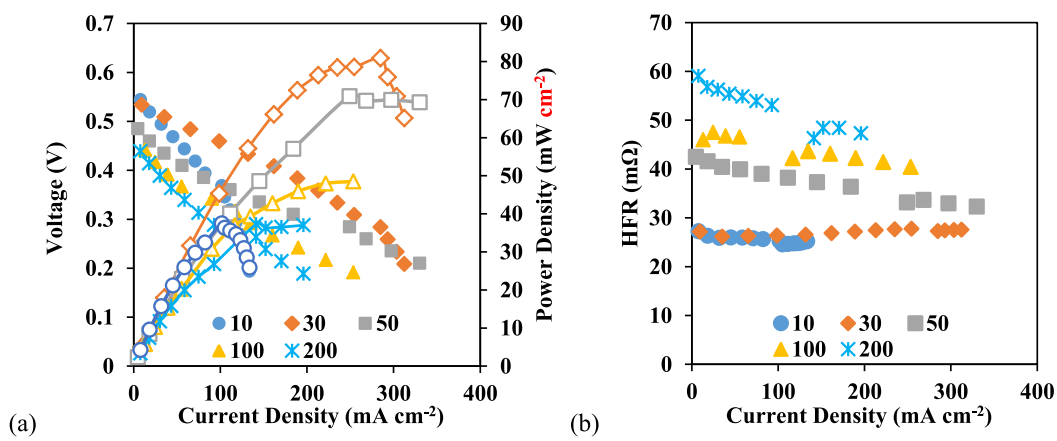

Fig. 5. (a) Polarization and performance curves using various N_2 flow rates and (b) corresponding HFR.

for the 1 mol/L (3.2 wt%) fuel is 186.9 mA cm^{-2} and drastically increases to 860.3 mA cm^{-2} when 25 wt% is supplied. This is clear evidence that the MCO is the limiting factor in high-concentration liquid feed supplies, despite the presence of water in the 25 wt% fuel and decreased flow rate.

3.2. Liquid feed versus vapor feed

Vapor feed supplies in a DMFC are advantageous due to the improved mass diffusivity of methanol in a vapor phase compared to a liquid phase. This allows for faster reaction kinetics of the MOR, and improved behavior of the two-phase flow in the anode channel, allowing adequate removal of generated CO_2, which allows fresh fuel and liquid water to react. Whereas in LFDMFCs, the two-phase interaction between liquid water/methanol and CO_2 gas inhibits the removal of CO_2 and the flow of fresh fuel [37]. Likewise, highly concentrated fuels can be utilized in VFDMFCs, improving both efficiency and energy density compared to dilute fuels. To explore this, all MEAs were evaluated using a liquid-fed 3.2 wt% solution and a vapor-fed 100 % pure methanol solution. Fig. 4 shows the results of the baseline tests of an MEA with no added WML and their resulting high-frequency resistance (HFR).

These results highlight the effect of liquid feed versus vapor feed supply techniques. The liquid feed system achieves a PPD of 109.4 mW cm^{-2} at a current density of 359.3 mA cm$^{-2,}$ and the vapor feed system achieves 80.2 mW cm^{-2} at a current density of 274.5 mA cm^{-2}, shown in Fig. 4**a**. Despite pure methanol being used as a fuel, the vapor feed supply shows impressive performance compared to the liquid feed supply. It can also be seen that the average HFR increased from 19 mΩ to 32 mΩ with the use of a vapor feed supply from the alcohol vapors rapidly drying the PEM and lack of adequate water generation at low current densities Fig. 4**b**.

3.3. Flow rate

The effect of the N_2 flow rate can have a significant impact on the performance of the vapor feed DMFC. To study this, performance scans were conducted using the N_2 flow rates of 10, 30, 50, 100, and 200 mL min^{-1}. Fig. 5**a** shows that the strongest performance occurs with 30 mL min^{-1} with a PPD of 80.9 mW cm^{-2} at a current density of 284.9 mA cm^{-2}. At 10 mL min^{-1}, the PPD decreases dramatically to 37.5 mW cm^{-2}, due to the insufficient fuel supply to achieve reasonable current density. At a flow rate of 50 mL min^{-1}, the performance decreases, compared to 30 mL min^{-1}, which is also evident by the increased HFR. As the HFR rises, the water retention of the PEM decreases. This is likely due to the accelerated drying of the PEM from the high N_2 supply rate causing increased removal of crucial water for the PEM to maintain ionic conductivity and for the MOR. Fig. 5**b** illustrates the strong relation between HFR increase of ≈35 to ≈45 and ≈50 mΩ for N_2 flow rates of 50, 100, and 200 mL min$^{-1,}$ respectively.

While Fig. 5**a-b** depicts the impact of the N_2 flow rate on performance, the impact of the N_2 flow rate on the MCO rate was also studied. For each flow rate, the fuel cell was held at OCV for 1 h to allow the

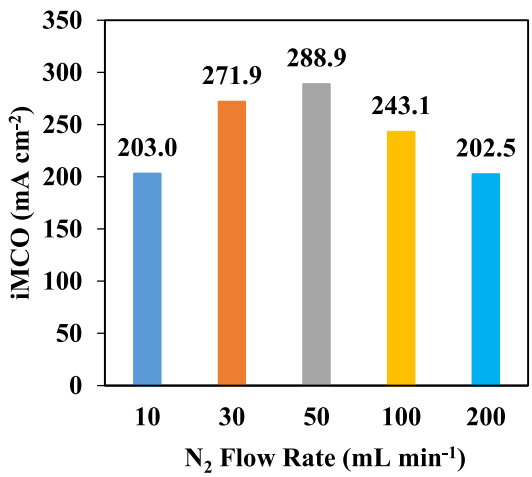

Fig. 6. Methanol crossover current density at multiple N_2 flow rates under OCV.

Table 1
Stochiometric ratio value for a variety of flow rates.

Flow Rate (mL min^{-1})	$\dot{Q}_{MeOHSupply}$ (mol/s)	$\dot{Q}_{MeOHConsumption}$ (mol/s)	$SR_{Theoretical\ Vap}$
10	1.06×10^{-6}	8.64×10^{-7}	1.2
30	3.19×10^{-6}	8.64×10^{-7}	3.7
50	5.32×10^{-6}	8.64×10^{-7}	6.2
100	1.06×10^{-5}	8.64×10^{-7}	12.3
200	2.13×10^{-5}	8.64×10^{-7}	24.7

sensor to respond and produce a stable value. The remaining 20 min of data were averaged. Using **Eqs. 15–16**, Fig. 6 shows the relationship between flow rate and i_{MCO}.

Notably, the flow rate shows the same correlation between performance and the crossover current density. The crossover current density was 203, 271.9, 288.9, 243.1, and 202.5 mA cm^{-2} for flow rates of 10, 30, 50, 100 and 200 mL min^{-1} of flow. The crossover rates increase with a flow rate between 10 and 50 mL min^{-1} but decrease as the flow rate exceeds 50 mL min^{-1}. This is due to the increased supply of N_2 in the fuel bottle, which decreases the evaporation rate of methanol, decreasing its supply, and increasing the N_2 flow into the cell. Table 1 shows the $SR_{Theoretical\ Vap}$ assuming a fixed current density of 100 mA cm^{-2}.

The $SR_{Theoretical\ Vap}$ increases rapidly with methanol supply due to its heavy dependence on our given anode volumetric flow rate. The $SR_{Theoretical\ Vap}$ will be vital for determining an appropriate flow rate at a fixed current density to improve efficiency and energy density. Once again, having an $SR_{Theoretical\ Vap}$ as exactly 1 at any instance would mean our supply rate is sufficient compared to our consumption rate to avoid fuel starvation. Conversely, an $SR_{Theoretical\ Vap}$ between 1 and 2 would reduce an oversupply of fuel, drastically improving fuel efficiency and energy density. This will be further explored in ***Section 3.5 Consumption Tests***.

3.4. Vapor feed concentration

The significance of using pure methanol as a fuel is that it has the highest gravimetric energy density when compared to dilute solutions The following are vapor feed tests conducted at 30 mL min^{-1} of N_2 flow and 200 mL min^{-1} of 100 % RH air. As seen in Fig. 5**a** **30** mL min^{-1} N_2 flow rate yielded the best results when using pure methanol as a fuel, hence the flow rate selection for these tests. In Fig. 7**a** the peak power density increases from 15.9 to 53.5, 60.7, and 74.6 mW cm^{-2} at fuel concentrations of 25 wt%, 50 wt%, 75 wt%, and 100 wt% respectively. Pure methanol fuel provides the highest power density at a current density of 269.5 mA cm^{-2} while maintaining an average internal resistance of 27.1 mΩ.

Pure methanol performs the best due to the sufficient supply of vaporized methanol. The supplied rate of methanol is lower at lower concentrations due to water vapor in the supply. Although Fig. 7**b** shows low and stable ohmic resistance for each fuel concentration, indicating adequate water supply, the limiting factor comes from the lack of methanol to sustain the MOR. Table 2 depicts how the water supply at lower concentrations is higher than the methanol supply. Hence the $SR_{Theoretical\ Vap}$ for 25 wt% and 50 wt% are low, 0.29 and 0.66, respectively. For the 75 wt% fuel, an $SR_{Theoretical\ Vap}$ above 1 at 200 mA cm^{-2} is achieved, but it still lacks performance compared to the pure methanol fuel. It can also be noted that there is a fluctuation in the power density curve for the 75 wt% fuel. This is due to the buildup and removal of excess water generated at higher current densities. This behavior has been observed by others when testing both hydrogen and methanol fuel cells at a fixed current for an extended period of time [38,39] The partial pressure ($P_{Partial}$) of water vapor at this temperature and concentration increases the water supply but still limits the supply of fresh fuel. Likewise, the remaining $P_{Partial}$ of the system is the N_2, which provides no value to the reaction.

Furthermore, the raw data used to calculate i_{MCO} is seen in Fig. 8**a** to understand the influence of concentration on the crossover rate (Fig. 8**b**). Similarly to previous i_{MCO} tests, the cell was held at OCV for 1 h at a flow rate of 30 mL min^{-1} to ensure steady state generation of CO_2. After completion of each test, the data collected in the final 20 min was

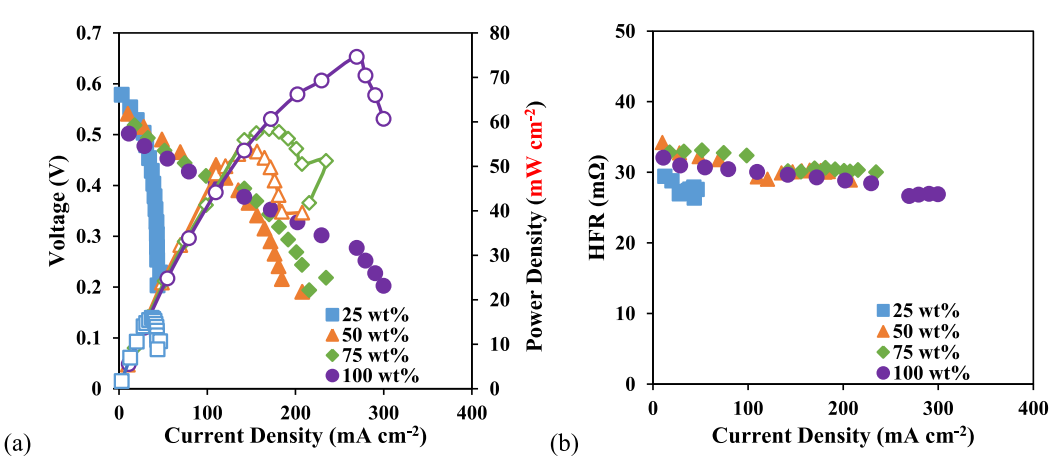

Fig. 7. Various weight percent concentrations of vapor feed methanol (a) polarization and performance scans and (b) HFR.

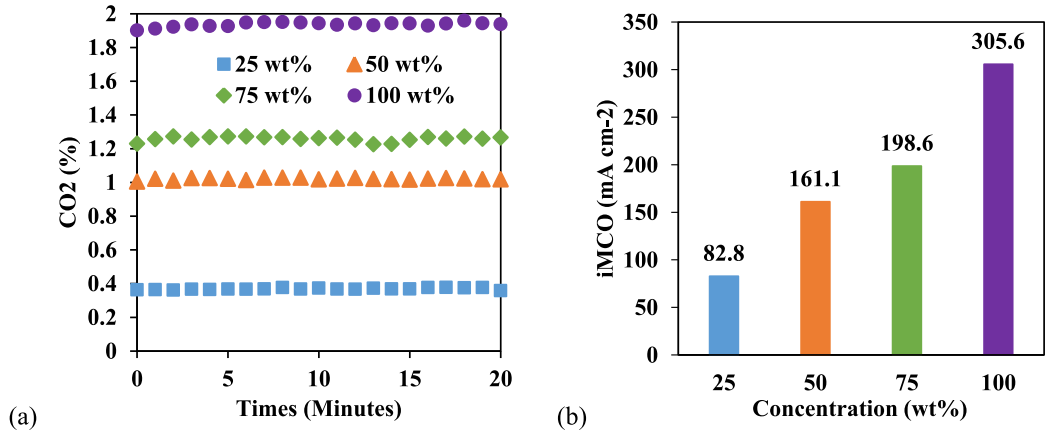

Fig. 8. The molar fraction of CO_2 (a) and i_{MCO} (b) under an N_2 flow rate of 30 mL min^{-1} and OCV conditions for multiple vapor-feed fuel concentrations.

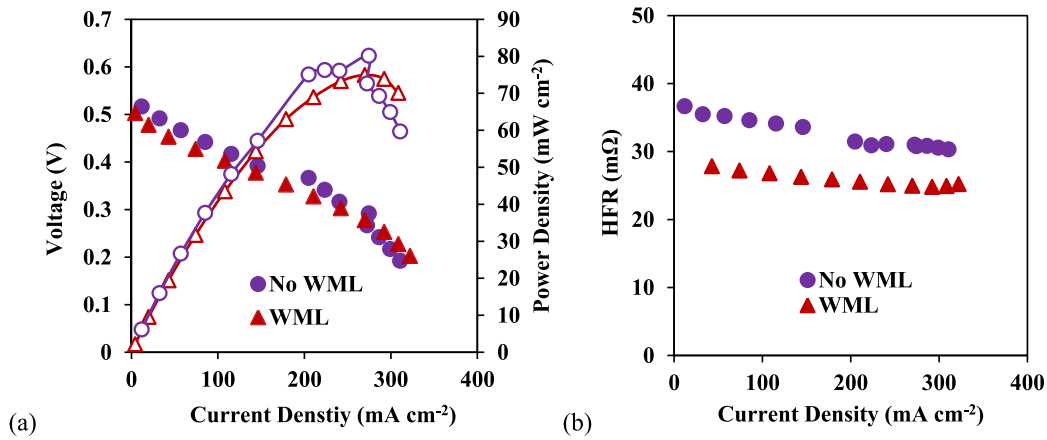

Fig. 9. Baseline testing (a) performance and (b) HFR of the VFDMFC with and without a WML at 60 °C using pure methanol at a N_2 flow rate of 30 mL min^{-1}.

averaged and used as the CO_2 concentration value for the i_{MCO} calculation. The 25 wt% fuel has a methanol supply of 5.04 × 10^{-7} mol/s and a water vapor supply of 3.27 × 10^{-6} mol/s, indicating that the supply rate of water vapor is an order of magnitude higher than our fuel supply. This leads to a low HFR (Fig. 7**b**) of 27.6 mΩ, but a low power density of 24.8 mW cm^{-2} due to fuel starvation. At a concentration of 50 wt%, the performance improves to a peak power density of 53.2 mW cm^{-2}. The supply rate of methanol increases to 1.15 × 10^{-6} mol/s and the water supply rate decreases to 2.49 × 10^{-6} mol/s.

The DMFC experiences i_{MCO} of 82.8, 161.1, 198.6, and 305.6 mA cm^{-2} at concentrations of 25 wt%, 50 wt%, 75 wt%, and 100 wt%, respectively. The crossover increases proportionally as the concentration increases. Considering the supply rate of methanol increases, the crossover rate also increases from the higher methanol $P_{Partial}$.

3.5. Consumption tests

This study quantitatively measured the impact of the WML on the crossover rate for the DMFC through a series of consumption tests. Initially, baseline tests were conducted to show performance similarities between the MEA with a WML and without Fig. 9.

The non-WML test performed slightly higher than the test with a WML. The PPD is 80.2 mW cm^{-2} at a current density of 274.5 mA cm^{-2} for the non-WML case. The WML case achieved 74.9 mW cm^{-2} at a current density of 269.8 mA cm^{-2}. The limiting current density was similar at 310.7 mA cm^{-2} and 308.6 mA cm^{-2} for the non-WML and WML cases, respectively. Notably, the average HFR decreased from 32.6 mΩ to 25.9 mΩ, indicating the WML's influence on water retention in the PEM. As mentioned in ***Section 2.4***, the flow rate selections come from the polarization curves generated in ***Section 3.3*** and the $SR_{Theoretical\ Vap}$. In an ideal case, the SR_{Tested} would be fixed at a value of 1, allowing perfect supply and consumption rates. However, this is not the case during actual operation, as the consumption rate can fluctuate slightly. Therefore, an $SR_{Theoretical\ Vap}$ above 1 would be ideal to mitigate any effects of consumption fluctuations. Likewise, as seen in ***Section 3.3*** the 10 mL min^{-1} flow rate showed low performance with a PPD of 37.5 mW cm^{-2} at a current density of 101.8 mA cm^{-2}. While this flow rate achieved moderate current density to run at a fixed 100 mA cm^{-2}, the voltage drops at current densities beyond the peak, and the cell reaches its limiting current density much quicker than other flow rates. This flow rate would reduce cell efficiency and, in turn, reduce energy density. The $SR_{Theoretical\ Vap}$ at 10 mL min^{-1} and a fixed current density of 100 mA cm^{-2} is 1.22. While this seems appealing, the issue of fuel starvation could cause issues when running at 100 mA cm^{-2}, as evident through the polarization curve in ***Section 3.3***. The SR_{Tested} will vary, given the operating conditions are not always ideal. Therefore, selecting a flow rate of 15 mL min^{-1}, slightly higher than the previous flow rate, would yield an $SR_{Theoretical\ Vap}$ of 1.85 and reduce the potential for fuel starvation. Likewise, for the 200 mA cm^{-2} consumption test case of 25 mL min^{-1} was selected due to its ability to prevent fuel starvation. Recalling the strong influence of current density on the consumption rate, the $SR_{Theoretical\ Vap}$ is 1.54. Considering the superior performance at 30 mL min^{-2}, in Fig. 5**a, 25** mL min^{-1} allows for sufficient current density generation while reducing our supply rate to increase fuel and cell

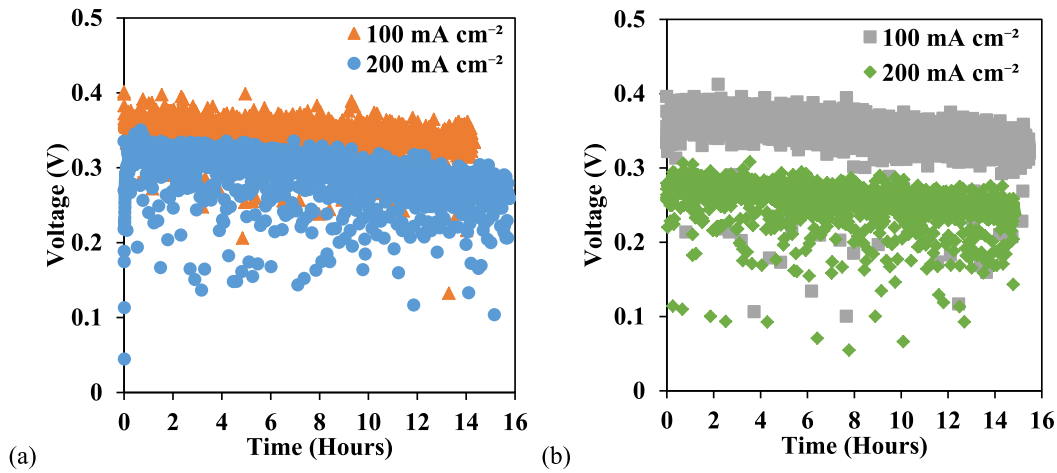

Fig. 10. Voltage result of consumption test with (a) and without (b) a WML at 100 mA cm^{-2} and 200 mA cm^{-2}.

Table 2
The stoichiometric ratio, saturation, and partial pressure of each fuel concentration at a fixed current density of 200 mA cm^{-2} at room temperature (22 °C).

Concentration (wt%)	Substance	P_{Sat} (kPa)	$P_{Partial}$ (kPa)	$\dot{Q}_{MeOHSupply}$ (mol/s)	$\dot{Q}_{MeOHConsumption}$ (mol/s)	$SR_{Theoretical\ Vap}$
25	MeOH	14.45	2.28	5.04×10^{-7}	1.73×10^{-6}	0.29
	H_2O	2.64	2.22	3.27×10^{-6}	–	
50	MeOH	14.45	5.20	1.15×10^{-6}	1.73×10^{-6}	0.66
	H_2O	2.64	1.69	2.49×10^{-6}	–	
75	MeOH	14.45	9.06	2.00×10^{-6}	1.73×10^{-6}	1.16
	H_2O	2.64	0.98	3.88×10^{-6}	–	
100	MeOH	14.45	14.45	3.19×10^{-6}	1.73×10^{-6}	1.85

Table 3
Fuel efficiency, total efficiency, and Energy Density results of consumption tests with and without a WML at multiple current densities.

i (mA cm^{-2})	$SR_{Theoretical\ Vap}$	SR_{Tested}	WML	η_{fuel}(%)	η_{volt}(%)	η_{tot}(%)	U_{tot} (Wh kg$^{-1}_{MeOH}$)
100	1.8	2.2	No	44.7	28.7	12.8	783.5
200	1.5	1.8	No	55.2	21	11.6	705.9
100	1.8	2.0	Yes	48.8	28.8	14.1	857.6
200	1.5	1.7	Yes	59.0	24.1	14.2	867.7

efficiency. For the tests without a WML, the mass consumption was 2.24 and 5.36 g when run at 100 mA cm^{-2} and 200 mA cm^{-2}, respectively. For the tests with a WML, the mass consumption was 2.93 and 5.34 g when at 100 mA cm^{-2} and 200 mA^{-2}, respectively. With this, the $\dot{Q}_{MeOH\ TS}$ without a WML are 1.93×10^{-6} and 3.12×10^{-6} mol/s for 100 mA cm^{-2} and 200 mA cm^{-2} respectively. For cases with a WML, the $\dot{Q}_{MeOH\ TS}$ rates are 1.73×10^{-6} and 2.93×10^{-6} mol/s for 100 mA cm^{-2} and 200 mA cm^{-2} respectively. The $\dot{Q}_{MeOH\ Consumption}$ rates are 8.64×10^{-7} and 1.73×10^{-6} mol/s for 100 mA cm^{-2} and 200 mA cm^{-2} respectively. The voltage produced throughout the entire consumption test with a WML and without a WML is plotted in Fig. 10. It can be noted that there are fluctuations in the voltage throughout the length of each test. As mentioned in *Section 3.4*, this behavior has been observed by others when testing both hydrogen and methanol fuel cells at a fixed current density for an extended period. The V_{avg} for the WML cases, Fig. 10**a**, were 0.349 and 0.292 V at 100 mA cm^{-2} and 200 mA cm^{-2} respectively. For the non-WML cases in Fig. 9**b**, the V_{avg} was 0.348 and 0.254 V at 100 mA cm^{-2} and 200 mA cm^{-2} respectively. Using **Eqns 6 and 9–16**, Table 3 provides a detailed breakdown of the results for each consumption test.

Without a WML, U_{tot} is 783.5 and 705.9 Wh kg$^{-1}_{MeOH}$ at 100 mA cm^{-2} and 200 mA cm^{-2}, respectively. Including the WML increases η_{fuel} to 48.8 % and 59.0 % at 100 mA cm^{-2}, and 200 mA cm^{-2}, respectively. The

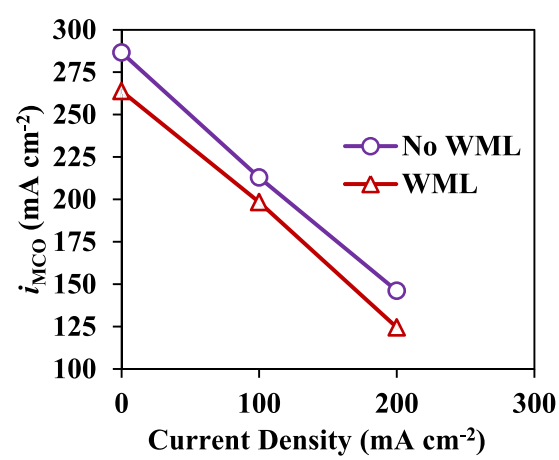

Fig. 11. Consumption test crossover current densities at OCV, 100 mA cm^{-2}, and 200 mA cm^{-2} with and without a WML.

η_{tot} increases to 14.1 % and 14.2 % at 100 mA cm^{-2}, and 200 mA cm^{-2}, respectively. With this, U_{tot} increased to 857.6 Wh kg$^{-1}_{MeOH}$ for 100 mA cm^{-2} with the WML due to the higher V_{avg} throughout the test prompted by a lower crossover rate of 198.4 mA cm^{-2} compared to 212.9 mA cm^{-2}

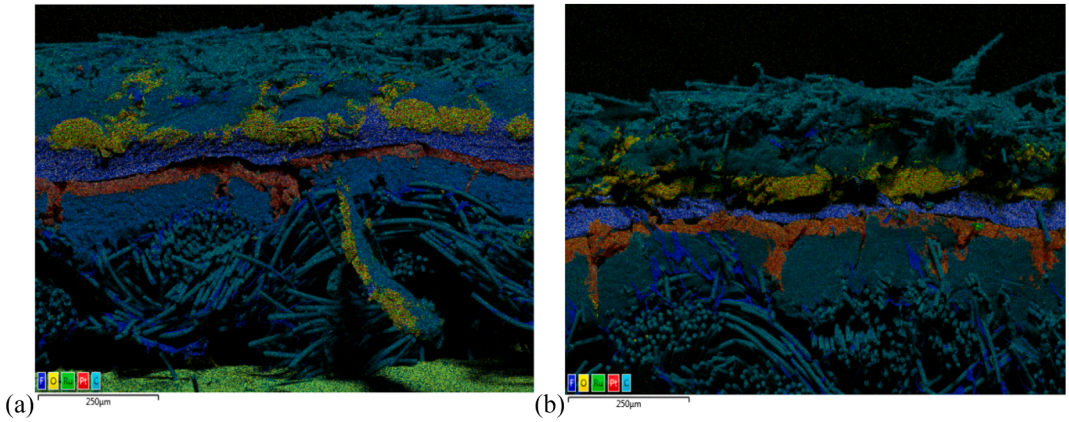

Fig. 12. (a) Layered SEM/EDS images of a fresh MEA prior to consumption testing and (b) layered SEM/EDS images of a post consumption MEA without a WML.

without a WML, a 7.1 % difference. For the 200 mA cm^{-2} case, U_{tot} increases more so with the inclusion of the WML to 867.7 Wh kg$^{-1}_{MeOH}$, yielding the best results of any configuration in these experiments. The Δ_{Mass} was slightly lower for the WML test at 200 mA cm^{-2} of 5.34 g compared to the case without a WML of 5.36 g with similar testing times. Fig. 11 shows the i_{MCO} for OCV, 100 mA cm^{-2}, and 200 mA cm^{-2} for consumption tests with and without a WML. The i_{MCO} is calculated the same as in ***Section 3.3,*** except the average CO_2% is taken from the entire consumption test.

The i_{MCO} at 200 mA cm^{-2} decreased from 146.1 mA cm^{-2} to 124.5 mA cm^{-2}, including the WML, a 16 % difference. While the MEA's outright performance is lower with the WML included Fig. 11 and Table 3 show that the WML is effective during long-term operation for reducing crossover and increasing efficiency. Pre and post consumption SEM images were taken to determine the most prevalent degradation form within the MEA.

It can be seen that in Fig. 12 that there is no major difference in the morphology of the anode or cathode catalyst layers when comparing a pre-consumption MEA and a post-consumption MEA. However, it can be noted that the post-consumption MEA in Fig. 12**b** suffered from ruthenium dissolution, on the righthand side of the image, where an agglomeration of ruthenium is detected within the cathode layer. Ruthenium dissolution in the anode is a common form of degradation within DMFCs [40,41] given ruthenium becomes unstable in the oxidative and low potential environment of the anode during the constant discharge. This causes the Ruthenium to diffuse across the PEM, reducing its proton conductivity, and decreases both the anode and cathode electrodes performance resulting in an overall decrease in cell performance.

4. Conclusions

This study reports the effectiveness of vapor feed DMFCs and how conditions such as flow rate, fuel concentration, and added WMLs influence performance, efficiency, and methanol crossover. The VFDFMC shows significant improvement in performance when using pure methanol and can be appropriately optimized to produce a high-energy density cell with the inclusion of a WML. Given the results, the following conclusions can be drawn:

1. Fuel concentration can significantly impact the LFDMFC and VFDMFC performance. However, when using pure methanol as a high-energy–density fuel, the VFDMFC obtained a similar performance with an LFDMFC using a dilute 1 M (3.2 wt%) fuel. A VFDMFC using pure methanol can obtain 80.2 mW cm^{-2} of PPD at a current density of 274.5 mA cm^{-2} compared to an LFDMFC using dilute 1 M fuel, which achieves 109.6 mW cm^{-2} at a current density of 359.3 mA cm^{-2}.
2. The flow rate of the inert-carrying gas can improve the performance of the VFDMFC when using pure methanol. The flow rate negatively affects performance when the supply rate of methanol is at the extreme of oversupply and undersupply. A 30 mL min^{-1} yields the highest PPD of 80.9 mW cm^{-2} with an equivalent methanol crossover of 271.9 mA cm^{-2}, in this study.
3. The performance of the VFDMFC increases with increasing methanol concentration. Low concentrations, 25 wt% and below, inhibit performance due to the high presence of water vapor in the fuel supply, which limits the availability of usable fuel. As the concentration increases from 50 wt% to 75 wt% and 100 wt%, performance increases as the presence of water vapor decreases and more fuel is available to react. However, as concentration increases, methanol crossover increases equally.
4. The addition of WMLs in the VFDMFC can increase both performance and efficiency due to the increased mass transfer resistance of water on the cathode, which increases water backflow. The addition of a WML increases energy density from 705.9 Wh kg^{-1} to 867.7 Wh kg^{-1} when discharged at 200 mA cm^{-2} for over 14 hrs. Likewise, the i_{MCO} decreases with WML addition from 146.2 mA cm^{-2} to 124.5 mA cm^{-2}, which contributes to improved water backflow, efficiency, and energy density.

In the future, the addition of FMLs could further increase performance, as discovered by Li et al. [28]. However, its structure would need to be optimized to suit the nature of the VFDMFC. Likewise, modifications to the PEM, as brought up by Metzger et al. [42] and Zhou et al. [43], could prove beneficial to further reduce the methanol crossover current density by decreasing the PEMs permeability to methanol vapor while maintaining proton conductivity. This design would also need to be adjusted for the VFDMFC to continue supporting water backflow through the PEM and to support anode reactions.

CRediT authorship contribution statement

Ryan Spragg: Writing – review & editing, Writing – original draft, Visualization, Validation, Methodology, Formal analysis, Data curation. **Xianglin Li:** Writing – review & editing, Supervision, Funding acquisition, Conceptualization.

Declaration of competing interest

The authors declare that they have no known competing financial interests or personal relationships that could have appeared to influence the work reported in this paper.

Data availability

Data will be made available on request.

Acknowledgments

The authors highly appreciate the support from the National Science Foundation (Award 1941083 and 2329821). Some material is based upon work supported by the U.S. Department of Energy's Office of Energy Efficiency and Renewable Energy (EERE) under the Hydrogen and Fuel Cell Technologies Office, Award Number DE-EE0008440. This study also utilized materials and devices in the Institute of Materials Science & Engineering (IMSE) at WashU and we acknowledge the partial financial support from the IMSE.

References

[1] Manthiram A. An outlook on lithium ion battery technology. ACS Cent Sci 2017;3:1063–9. https://doi.org/10.1021/acscentsci.7b00288.
[2] Rafiee A. Modelling and optimization of methanol synthesis from hydrogen and CO2. J Environ Chem Eng 2020;8:104314. https://doi.org/10.1016/j.jece.2020.104314.
[3] Møller KT, Jensen TR, Akiba E, Li H. Hydrogen - a sustainable energy carrier. Prog Nat Sci Mater Int 2017;27:34–40. https://doi.org/10.1016/j.pnsc.2016.12.014.
[4] Ahmed AA, Al Labadidi M, Hamada AT, Orhan MF. Design and utilization of a direct methanol fuel cell. Membranes 2022;12:1266. https://doi.org/10.3390/membranes12121266.
[5] Miao Z, Hu B, He Y-L, et al. A liquid-vapor two-phase model of direct methanol fuel cells with platinum group metal-free cathode catalyst. J Electrochem Energy Convers Storage 2021;18:040904. https://doi.org/10.1115/1.4051209.
[6] Rice J, Faghri A. Analysis of a passive vapor feed direct methanol fuel cell. Int J Heat Mass Transf 2008;51:948–59. https://doi.org/10.1016/j.ijheatmasstransfer.2007.08.025.
[7] Li X, Faghri A. Review and advances of direct methanol fuel cells (DMFCs) part I: design, fabrication, and testing with high concentration methanol solutions. J Power Sources 2013;226:223–40. https://doi.org/10.1016/j.jpowsour.2012.10.061.
[8] Abdelkareem MA, Allagui A, Sayed ET, et al. Comparative analysis of liquid versus vapor-feed passive direct methanol fuel cells. Renew Energy 2019;131:563–84. https://doi.org/10.1016/j.renene.2018.07.055.
[9] Mallick RK, Thombre SB, Shrivastava NK. Vapor feed direct methanol fuel cells (DMFCs): a review. Renew Sustain Energy Rev 2016;56:51–74. https://doi.org/10.1016/j.rser.2015.11.039.
[10] Eccarius S, Krause F, Beard K, Agert C. Passively operated vapor-fed direct methanol fuel cells for portable applications. J Power Sources 2008;182:565–79. https://doi.org/10.1016/j.jpowsour.2008.03.091.
[11] Kim H. Passive direct methanol fuel cells fed with methanol vapor. J Power Sources 2006;162:1232–5. https://doi.org/10.1016/j.jpowsour.2006.08.006.
[12] Li X, Faghri A, Xu C. Structural optimization of the direct methanol fuel cell passively fed with a high-concentration methanol solution. J Power Sources 2010;195:8202–8. https://doi.org/10.1016/j.jpowsour.2010.06.041.
[13] Xu Q, Zhang W, Zhao J, et al. Effect of air supply on the performance of an active direct methanol fuel cell (DMFC) fed with neat methanol. Int J Green Energy 2018;15:181–8. https://doi.org/10.1080/15435075.2018.1431547.
[14] Moreno-Zuria A, Rivera JG, Chávez-Ramírez AU, Mohamedi M. Filter paper as electrolyte flow transport using vaporized methanol as fuel in a microfluidic fuel cell: experimental and numerical simulation. DeCarbon 2024;4:100046. https://doi.org/10.1016/j.decarb.2024.100046.
[15] Xu C, Faghri A. Mass transport analysis of a passive vapor-feed direct methanol fuel cell. J Power Sources 2010;195:7011–24. https://doi.org/10.1016/j.jpowsour.2010.05.003.
[16] Chen R, Zhao TS. A novel electrode architecture for passive direct methanol fuel cells. Electrochem Commun 2007;9:718–24. https://doi.org/10.1016/j.elecom.2006.11.004.
[17] Li X, Faghri A. Effect of the cathode open ratios on the water management of a passive vapor-feed direct methanol fuel cell fed with neat methanol. J Power Sources 2011;196:6318–24. https://doi.org/10.1016/j.jpowsour.2011.03.047.
[18] Zhang Y, Yuan W, Hou C, et al. Improved vapor-feed direct methanol fuel cell by hydrophobic/hydrophilic composite catalyst layers via kelvin equation. ACS Sustain Chem Eng 2024;12:3680–90. https://doi.org/10.1021/acssuschemeng.3c07231.
[19] Xu C, Faghri A, Li X. Improving the water management and cell performance for the passive vapor-feed DMFC fed with neat methanol. Int J Hydrog Energy 2011;36:8468–77. https://doi.org/10.1016/j.ijhydene.2011.03.115.
[20] Zhang Z, Yuan W, Wang A, et al. Moisturized anode and water management in a passive vapor-feed direct methanol fuel cell operated with neat methanol. J Power Sources 2015;297:33–44. https://doi.org/10.1016/j.jpowsour.2015.07.097.
[21] Li B, Xie M, Ji H, et al. Optimization of cathode microporous layer materials for proton exchange membrane fuel cell. Int J Hydrog Energy 2021;46:14674–86. https://doi.org/10.1016/j.ijhydene.2021.01.169.
[22] Wang Z, Zhang X, Nie L, et al. Elimination of water flooding of cathode current collector of micro passive direct methanol fuel cell by superhydrophilic surface treatment. Appl Energy 2014;126:107–12. https://doi.org/10.1016/j.apenergy.2014.03.029.
[23] Zhao TS, Xu C, Chen R, Yang WW. Mass transport phenomena in direct methanol fuel cells. Prog Energy Combust Sci 2009;35:275–92. https://doi.org/10.1016/j.pecs.2009.01.001.
[24] Wu QX, Zhao TS. Characteristics of water transport through the membrane in direct methanol fuel cells operating with neat methanol. Int J Hydrog Energy 2011;36:5644–54. https://doi.org/10.1016/j.ijhydene.2011.01.145.
[25] Yuan W, Zhang Y, Zhang X, Zhang Y. Novel anode electrode structure with a fuel management layer for high-concentration passive direct methanol fuel cells. Energy Fuels 2024;38:5485–92. https://doi.org/10.1021/acs.energyfuels.3c05146.
[26] Zhang J, Yin G-P, Lai Q-Z, et al. The influence of anode gas diffusion layer on the performance of low-temperature DMFC. J Power Sources 2007;168:453–8. https://doi.org/10.1016/j.jpowsour.2007.03.027.
[27] Wu QX, Zhao TS, Chen R, An L. A sandwich structured membrane for direct methanol fuel cells operating with neat methanol. Appl Energy 2013;106:301–6. https://doi.org/10.1016/j.apenergy.2013.01.016.
[28] Li X, Miao Z, Marten L, Blankenau I. Experimental measurements of fuel and water crossover in an active DMFC. Int J Hydrog Energy 2021;46:4437–46. https://doi.org/10.1016/j.ijhydene.2020.11.027.
[29] Xu C, Faghri A, Li X, Ward T. Methanol and water crossover in a passive liquid-feed direct methanol fuel cell. Int J Hydrog Energy 2010;35:1769–77. https://doi.org/10.1016/j.ijhydene.2009.12.055.
[30] Jewett G, Faghri A, Xiao B. Optimization of water and air management systems for a passive direct methanol fuel cell. Int J Heat Mass Transf 2009;52:3564–75. https://doi.org/10.1016/j.ijheatmasstransfer.2009.03.006.
[31] Mench MM. Fuel cell engines. Hoboken, N.J.: John Wiley & Sons; 2008.
[32] Bayramoğlu M, Ciğeroğlu Z, Kazan ES. Experimental evaluation of the efficiency performance of the DMFC. Environ Prog Sustain Energy 2020;39:e13454.
[33] Cao J, Wang L, Song L, et al. Novel cathodal diffusion layer with mesoporous carbon for the passive direct methanol fuel cell. Electrochim Acta 2014;118:163–8. https://doi.org/10.1016/j.electacta.2013.11.140.
[34] Seo SH, Lee CS. A study on the overall efficiency of direct methanol fuel cell by methanol crossover current. Appl Energy 2010;87:2597–604. https://doi.org/10.1016/j.apenergy.2010.01.018.
[35] Schaffer T, Hacker V, Hejze T, et al. Introduction of an improved gas chromatographic analysis and comparison of methods to determine methanol crossover in DMFCs. J Power Sources 2005;145:188–98. https://doi.org/10.1016/j.jpowsour.2004.11.074.
[36] Han J, Liu H. Real time measurements of methanol crossover in a DMFC. J Power Sources 2007;164:166–73. https://doi.org/10.1016/j.jpowsour.2006.09.105.
[37] Scott K, Taama WM, Argyropoulos P. Engineering aspects of the direct methanol fuel cell system. J Power Sources 1999;79:43–59. https://doi.org/10.1016/S0378-7753(98)00198-0.
[38] Wan N. Durability study of direct methanol fuel cell under accelerated stress test. J Power Sources 2023;556:232470. https://doi.org/10.1016/j.jpowsour.2022.232470.
[39] Wahdame B, Candusso D, Francois X, et al. Comparison between two PEM fuel cell durability tests performed at constant current and under solicitations linked to transport mission profile. Int J Hydrog Energy 2007;32:4523–36. https://doi.org/10.1016/j.ijhydene.2007.03.013.
[40] Piela P, Eickes C, Brosha E, et al. Ruthenium crossover in direct methanol fuel cell with Pt-Ru black anode. J Electrochem Soc 2004;151:A2053. https://doi.org/10.1149/1.1814472.
[41] Lo Vecchio C, Serov A, Dicome M, et al. Investigating the durability of a direct methanol fuel cell equipped with commercial Platinum Group Metal-free cathodic electro-catalysts. Electrochim Acta 2021;394:139108. https://doi.org/10.1016/j.electacta.2021.139108.
[42] Metzger N, Vlassiouk I, Smirnov S, et al. Experimental studies of graphene-coated polymer electrolyte membranes for direct methanol fuel cells. J Electrochem Energy Convers Storage 2023;20:020903. https://doi.org/10.1115/1.4056269.
[43] Zhou J, Cao J, Zhang Y, et al. Overcoming undesired fuel crossover: Goals of methanol-resistant modification of polymer electrolyte membranes. Renew Sustain Energy Rev 2021;138:110660. https://doi.org/10.1016/j.rser.2020.110660.